

Focal and Efficient IOU Loss for Accurate Bounding Box Regression

Yi-Fan Zhang^{a,b}, Weiqiang Ren^c, Zhang Zhang^{a,b,c}, Zhen Jia^{a,b}, Liang Wang^{a,b}, and Tieniu Tan^{a,b}

^aCRIPAC & NLPR, CASIA, Beijing, China

^bUniversity of Chinese Academy of Sciences, Beijing, China

^cHorizon Robotics.

Abstract

In object detection, bounding box regression (BBR) is a crucial step that determines the object localization performance. However, we find that most previous loss functions for BBR have two main drawbacks: (i) Both ℓ_n -norm and IOU-based loss functions are inefficient to depict the objective of BBR, which leads to slow convergence and inaccurate regression results. (ii) Most of the loss functions ignore the imbalance problem in BBR that the large number of anchor boxes which have small overlaps with the target boxes contribute most to the optimization of BBR. To mitigate the adverse effects caused thereby, we perform thorough studies to exploit the potential of BBR losses in this paper. Firstly, an Efficient Intersection over Union (EIOU) loss is proposed, which explicitly measures the discrepancies of three geometric factors in BBR, i.e., the overlap area, the central point and the side length. After that, we state the Effective Example Mining (EEM) problem and propose a regression version of focal loss to make the regression process focus on high-quality anchor boxes. Finally, the above two parts are combined to obtain a new loss function, namely Focal-EIOU loss. Extensive experiments on both synthetic and real datasets are performed. Notable superiorities on both the convergence speed and the localization accuracy can be achieved over other BBR losses.

Keywords:

Object detection, loss function design, hard sample mining.

1. Introduction

Object detection, which includes two sub-tasks: object classification and object localization, is always one of the most fundamental problems in computer vision. Current state-of-the-art object detectors (e.g., Cascade R-CNN [2], Mask R-CNN [10], Dynamic R-CNN [28], and DETR [3]) rely on a bounding box regression (BBR) module to localize objects. Based on this paradigm, a well-designed loss function is of vital importance for the success of BBR. So far, most of loss functions for BBR fall into two categories:

- ℓ_n -norm losses can be unified as Eq. (1).

$$L(x) = \begin{cases} f(x), & \text{if } |x| < \beta, \\ g(x), & \text{otherwise,} \end{cases} \quad (1)$$

where x is the difference between the predicted box and the target box. Traditional SmoothL1 loss [8] can be formed as $\beta = 1$, $f(x) = 0.5|x|^2/\beta$ and $g(x) = |x| - 0.5\beta$. ℓ_n -norm losses have been criticized for not only ignoring the correlations in BBR variables (x, y, w, h) but also the intrinsic bias to the large bounding boxes (due to the unnormalized form) [27]. However, previous IOU-based losses, e.g., CIOU and GIOU, cannot measure the discrepancies between target box and anchors efficiently, which leads to slow convergences and inaccurate localizations in optimizations of BBR models as illustrated in Figure 1.

- Intersection over Union (IOU)-based losses can be unified as Eq. (2).

$$L(B, B^{gt}) = 1 - \frac{|B \cap B^{gt}|}{|B \cup B^{gt}|} + R(B, B^{gt}), \quad (2)$$

where B and B^{gt} are the predicted box and the target box. The penalty term $R(B, B^{gt})$ is designed for the complementary benefit to the original IOU cost. These losses jointly regress all the BBR variables as a whole unit. They are also normalized and insensitive to the scales of bounding boxes. However, most of them suffer from the slow convergence speed and inaccurate localizations. What's more, the existing IOU-based losses neglect the importance of the informative anchor boxes.

In this paper, we take thorough studies to exploit the potential of current BBR losses for accurate object detections. Firstly, an Efficient IOU loss (EIOU) is proposed to improve the convergence speed and localization accuracy, which uses an additional penalty term $R(B, B^{gt})$ to explicitly measure the discrepancies of three key geometric factors in BBR, including the overlap area, the central point and the side length. Secondly, we state the Effective Example Mining (EEM) problem in BBR. Inspired by the focal loss [15] originally applied to measure the classification errors, we design a regression version of focal loss to enhance the contributions of high-quality anchor boxes with large IOUs in the optimization process of BBR models. Finally,

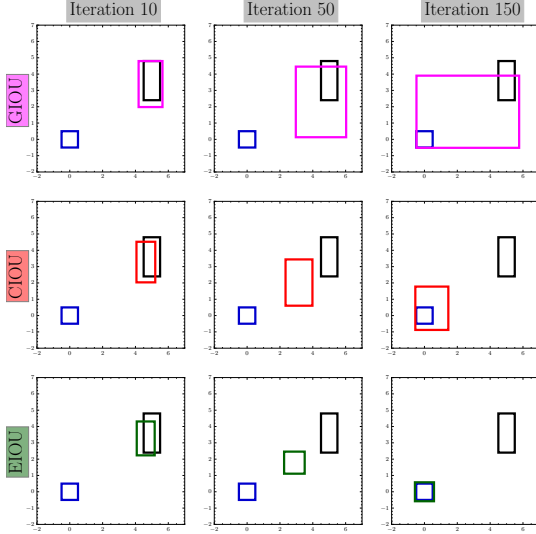


Figure 1:

the two proposed methods are combined as a new BBR loss function, namely Focal-EIOU, for efficient and accurate object detection. The effectiveness and advantages of the proposed loss functions are validated by extensive evaluations on both the synthetic and real datasets. Furthermore, when we incorporate the Focal-EIOU loss with several state-of-the-art object detection models, including Faster R-CNN [23], Mask R-CNN [10], RetinaNet [15], ATSS [29], PAA [12] and DETR [3], consistent and significant improvements of detection accuracy can be achieved on the large scale COCO 2017 dataset [16], which illustrates the promising potentials of the proposed loss function.

The contributions of this paper can be summarized as follows:

1. Considering the flaws of the IOU-based losses and ℓ_n -norm losses, we propose an efficient IOU loss to tackle the dilemma of existing losses and obtain a faster convergence speed and superior regression results.
2. Considering the imbalance between high and low-quality anchor boxes in BBR, we design a regression version of focal loss to enhance contributions of the most promising anchor boxes in model optimization while suppress the irrelevant ones’.
3. Extensive experiments have been conducted on both synthetic and real data. Outstanding experimental results validate the superiority of the proposed methods. Detailed ablation studies exhibit the effects of different settings of loss functions and parameter values .

2. Related Work

2.1. Loss Functions for BBR

The regression of bounding boxes is a crucial step in object detection. It aims to refine the location of a predicted bounding box based on the initial proposal or the anchor box. Till now,

BBR has been used on most of the recent detection methods [6, 9, 23, 26, 1, 18, 7].

Researchers have spent many efforts in designing loss functions for BBR. YOLO v1 [22] proposes to predict the square root of the bounding box size to remedy scale sensitivity. Fast R-CNN [8] and Faster R-CNN [23] use SmoothL1 loss function, which is a robust ℓ_1 loss that is less sensitive to outliers than the ℓ_2 loss used in R-CNN [9] and SPPNet [11]. The Dynamic SmoothL1 Loss [28] has the same $f(x)$ and $g(x)$ (in Eq.(1)) as the SmoothL1 loss, while it dynamically controls the shape of the loss function to gradually focus on high-quality anchor boxes. The BalanceL1 loss [19] is proposed to redefine $f(x)$ and $g(x)$ to obtain larger gradients for inliers, but the gradients of outliers are not influenced. However, the ℓ_n -norm loss functions mostly assume the four variables of bounding boxes (x, y, w, h) are independent, which is inconsistent with reality. To address the above problems, the IOU [27] loss is proposed and it achieves the superior performance on FDDb benchmark at that time. Further, the Generalized IOU (GIOU) [24] loss is proposed to address the weaknesses of the IOU loss, i.e., the IOU loss will always be zero when two boxes have no intersection. Recently, the Distance IOU and Complete IOU have been proposed [30], where the two losses have faster convergence speed and better performance. Pixels IOU [5] increases both the angle and IOU accuracy for oriented bounding boxes regression.

We address the weakness of existing loss functions, then propose an efficient loss function for object detection.

2.2. Effective Example Mining

One stage detectors suffer from the imbalance issue, such as inter-class imbalance between foreground and background examples. To address this challenge, SSD [17] adopts hard negative mining, which only keeps a small set of hard background examples for training. Focal loss [15] re-weights the background and foreground examples such that the hard examples are assigned with large weights. OHEM [25] presents a simple yet surprisingly effective online hard example mining algorithm for training region-based ConvNet detectors. The AP loss [4] and DR loss [21] transform the classification task into the sorting task, to avoid the imbalance between negative and positive examples. In BBR, the imbalance problem still exists, where most anchor boxes have small overlaps with target boxes. While only a small quantity of boxes are most informative for object localization. The most irrelevant boxes with small IOUs will produce excessively large gradients that are inefficient for the training of regression models. Libra R-CNN [19] and Dynamic R-CNN [28] suggest that a well-regressed bounding box should contribute more gradients in the model optimization process, based on which they revise the SmoothL1 loss to re-weight predicted bounding boxes.

However, the revised losses [28, 19] can only increase gradients of high-quality examples and cannot suppress the outliers’. Different from the above work, we design a regression version of focal loss to sufficiently exploit the most promising anchor boxes.

3. Efficient Intersection over Union Loss

In this section, we firstly analyze the drawbacks of existing popular loss functions and then propose the Efficient IOU loss.

3.1. Limitations of IOU-Based Losses

In this subsection, we analyze the flaws of three IOU-based loss functions, i.e., the IOU [27], GIoU [24] and CIOU [30] loss.

3.1.1. Limitations of IOU Loss

The IOU loss [27] for measuring similarity between two arbitrary shapes (volumes) $A, B \subseteq \mathbb{S} \in \mathbb{R}^n$ is attained by:

$$L_{IOU} = 1 - \frac{|A \cap B|}{|A \cup B|}, \quad (3)$$

which has some good properties, such as non-negativity, symmetry, triangle inequality and scale insensitivity. It has been proved to be a metric (by the mathematical definition [13]). However, it has two major drawbacks:

- If two boxes do not have any intersections, the IOU loss will be always zero, which cannot reflect the closeness between this two boxes correctly.
- The convergence speed of the IOU loss is slow.

3.1.2. Limitations of Generalized IOU Loss

The GIoU loss [24] loss is proposed to solve the drawbacks of the IOU loss and it is defined as follows,

$$L_{GIoU} = 1 - IOU + \frac{|C - (A \cup B)|}{|C|}, \quad (4)$$

where $A, B \subseteq \mathbb{S} \in \mathbb{R}^n$ are two arbitrary boxes. C is the smallest convex box $C \subseteq \mathbb{S} \in \mathbb{R}^n$ enclosing both A and B and $IOU = |A \cap B|/|A \cup B|$. The GIoU loss works when $|A \cap B| = 0$ while it still has two drawbacks:

- When $|A \cap B| = 0$, the GIoU loss intends to increase the bounding box's area, making it overlap the target box (see Figure 1), which is opposite to the intuition that decreasing the discrepancy of spatial positions.
- When $|A \cap B| > 0$, the area of $|C - A \cup B|$ is always a small number or equals zero (when A contains B , this term will be zero, vice versa). In such a case, the GIoU loss degrades to the IOU loss. As a consequence, the converge rate of the GIoU loss is still slow.

3.1.3. Limitations of Complete IOU Loss

The CIOU loss [30] considers three important geometric factors, i.e., the overlap area, the central point distance and the aspect ratio. Given a predicted box B and a target box B^{gt} , the CIOU loss is defined as follows.

$$L_{CIOU} = 1 - IOU + \frac{\rho^2(\mathbf{b}, \mathbf{b}^{gt})}{c^2} + \alpha v, \quad (5)$$

where \mathbf{b} and \mathbf{b}^{gt} denote the central points of B and B^{gt} respectively. $\rho(\cdot) = \|\mathbf{b} - \mathbf{b}^{gt}\|_2$ indicates the Euclidean distance. c is the diagonal length of the smallest enclosing box covering the two boxes. $v = \frac{4}{\pi^2} (\arctan \frac{w^{gt}}{h^{gt}} - \arctan \frac{w}{h})^2$ and $\alpha = \frac{v}{(1-IOU)+v}$ measure the discrepancy of the width-to-height ratio.

The gradient of v , w.r.t w and h , is calculated as follows.

$$\begin{aligned} \frac{\partial v}{\partial w} &= \frac{8}{\pi^2} (\arctan \frac{w^{gt}}{h^{gt}} - \arctan \frac{w}{h}) * \frac{h}{w^2 + h^2}, \\ \frac{\partial v}{\partial h} &= -\frac{8}{\pi^2} (\arctan \frac{w^{gt}}{h^{gt}} - \arctan \frac{w}{h}) * \frac{w}{w^2 + h^2}. \end{aligned} \quad (6)$$

In the previous work [30], experimental results show that both the converge speed and detection accuracy of the CIOU loss have a significant improvement, compared to previous loss functions. However, v in the last term of L_{CIOU} is still not well-defined, which slows down the convergence speed of CIOU from three aspects.

- In Eq. (5), v just reflects the discrepancy of aspect ratio, rather than the real relations between w and w^{gt} or h and h^{gt} . Namely, all the boxes with the property $\{(w = kw^{gt}, h = kh^{gt}) | k \in \mathbb{R}^+\}$ have $v = 0$, which is inconsistent with reality.
- In Eq. (6), we have $\frac{\partial v}{\partial w} = -\frac{h}{w} \frac{\partial v}{\partial h}$. $\frac{\partial v}{\partial w}$ and $\frac{\partial v}{\partial h}$ have opposite signs. Thus, at any time, if one of these two variables (w or h) is increased, the other one will decrease. It is unreasonable especially when $w < w^{gt}$ and $h < h^{gt}$ or $w > w^{gt}$ and $h > h^{gt}$.
- Since the v only reflects the discrepancy of aspect ratio, the CIOU loss may optimizes the similarity in a unreasonable way. As shown in Fig. 1, the scales of the target box are set as $w^{gt} = 1$ and $h^{gt} = 1$. The initial scales of the anchor box are set as $w = 1$ and $h = 2.4$. The anchor box's scales are regressed to $w = 1.64$ and $h = 2.84$ after 50 iterations. Here, the CIOU loss indeed increases the similarity of the aspect ratio, while it hinders the model from reducing the true discrepancy between (w, h) and (w^{gt}, h^{gt}) efficiently.

3.2. The Proposed Method

To address the above problems, we revise the CIOU loss and propose a more efficient version of IOU loss, i.e., the EIOU loss, which is defined as follows.

$$\begin{aligned} L_{EIOU} &= L_{IOU} + L_{dis} + L_{asp} \\ &= 1 - IOU + \frac{\rho^2(\mathbf{b}, \mathbf{b}^{gt})}{(w^c)^2 + (h^c)^2} + \frac{\rho^2(w, w^{gt})}{(w^c)^2} + \frac{\rho^2(h, h^{gt})}{(h^c)^2}, \end{aligned} \quad (7)$$

where w^c and h^c are the width and height of the smallest enclosing box covering the two boxes. Namely, we divide the loss function into three parts: the IOU loss L_{IOU} , the distance loss L_{dis} and the aspect loss L_{asp} . In this way, we can retain the profitable characteristics of the CIOU loss. At the same time, the EIOU loss directly minimizes the difference of the target box's and anchor box's width and height, which results in a faster converge speed and a better localization result. For a clear demonstration of the superiorities of the EIOU loss, we perform simulation experiments with synthetic data as presented in Section 5.3.

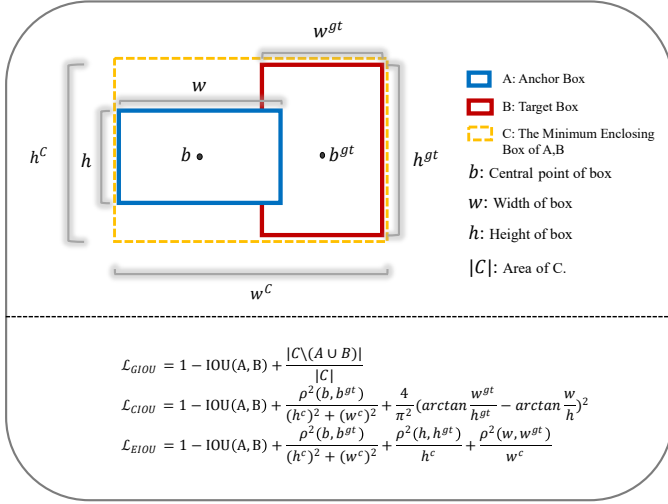


Figure 2:

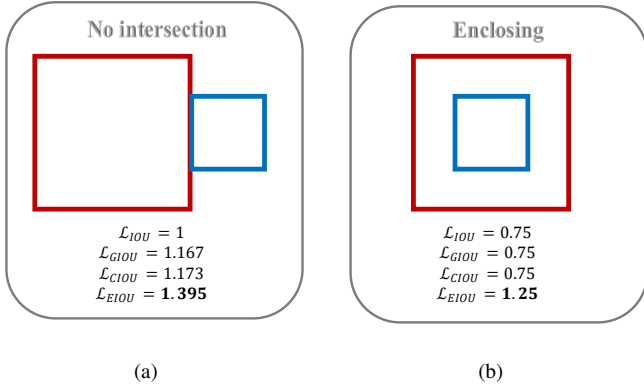


Figure 3:

4. Focal Loss For BBR

In BBR, the problem of imbalanced training examples also exists, i.e., the number of high-quality examples (anchor boxes) with small regression errors is much fewer than low-quality examples (outliers) due to the sparsity of target objects in images. Recent work [19] has shown that the outliers will produce excessively large gradients that are harmful to the training process. Thus, it is of vital importance that making the high-quality examples contribute more gradients to the network training process. As introduced in Section 2.2, recent studies [19, 28] have attempted to solve the above problem based on the SmoothL1 loss. In this section, we also start with the SmoothL1 loss and propose FocalL1 loss to increase the contribution of high-quality examples. Furthermore, we find that the simple method cannot be adapted to the IOU-based losses directly. Hence, we finally propose Focal-EIOU loss to improve the performance of the EIOU loss.

4.1. FocalL1 Loss

Firstly, we list the properties of the desirable loss function as follows.

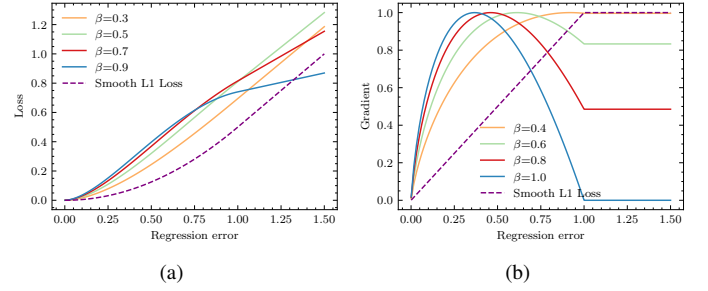


Figure 4: Curves for (a) loss and (b) gradient of our FocalL1 loss for bounding box regression.

1. When the regression error goes to zero, the gradient magnitude should have a limit of zero.
2. The gradient magnitude should increase rapidly around small regression errors and decrease gradually in the area of large regression errors.
3. There should be some hyper-parameters to control the degree of inhibition of low-quality examples flexibly.
4. With variant values of hyper-parameters, the family of gradient functions should have a normalized scale, e.g., $(0, 1]$, which facilitates the balancing between high-quality and low-quality examples.

According to the above conditions, as the change of the regression error of bounding box, we can assume an expected function curve of gradient magnitude, which is shown in Figure 5(a). The function is $-x \ln x$, satisfying the properties 1 and 2. Next, we construct a function family with a parameter β to control the shape of curves as shown in Figure 5(b). As β increases, the gradient magnitudes of outliers will be further suppressed. However, the gradient magnitudes of high-quality examples will also decrease, which is not what we expect. Thus, we add another parameter α to normalize the gradient magnitudes with different β into $[0, 1]$ as required by property 4. Finally, the family of gradient magnitude functions can be formulated as follows.

$$g(x) = \frac{\partial L_f}{\partial x} = \begin{cases} -\alpha x \ln(\beta x), & 0 < x \leq 1; 1/e \leq \beta \leq 1, \\ -\alpha \ln(\beta), & x > 1; 1/e \leq \beta \leq 1. \end{cases} \quad (8)$$

Here, the value range of β is obtained due to the following reasons. When $x \in (0, 1]$, $g''(x) = -\frac{\alpha}{x} \leq 0$, which means $g(x)$ is a concave function with a global maximal value. Solving $g'(x) = 0$, we can get $x^* = \frac{1}{e\beta}$. As $x^* \in (0, 1]$, $\frac{1}{e\beta} \in [0, 1] \rightarrow \beta \in [1/e, \infty]$. We also must ensure $\beta x \in (0, 1]$, then, $\beta \in [1/e, 1]$. To satisfy the property 4, we set the maximal value $f(x^*) = 1$ and get the relation between α and β : $\alpha = e\beta$. By integrating the gradient formulation above, we can get the FocalL1 loss for BBR,

$$L_f(x) = \begin{cases} -\frac{\alpha x^2 (2 \ln(\beta x) - 1)}{4}, & 0 < x \leq 1; 1/e \leq \beta \leq 1, \\ -\alpha \ln(\beta) x + C, & x > 1; 1/e \leq \beta \leq 1, \end{cases} \quad (9)$$

where C is a constant value. To ensure L_f in Eq. (9) is continuous at $x = 1$, we have $C = (2\alpha \ln \beta + \alpha)/4$.

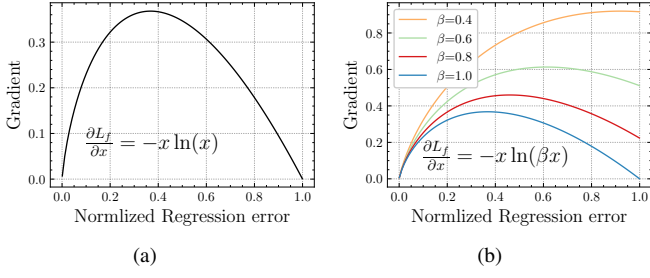


Figure 5: Possible gradient curves. (a) The gradient curve that we expect. (b) Use β to control the curves' shape.

Figure 4(b) shows the proposed FocalL1 loss can increase the value of inliers' gradients and suppress the value of outliers' gradients according to β . A larger β requires the inliers to have few regression errors and quickly suppresses the gradients' value of outliers. Similarly, in Figure 4(a) the blue curve denotes the maximal value of β . With the increase of regression error, the loss of the blue curve first increases rapidly and then tends to be stable. The orange curve with the minimal β value is growing faster and faster, reaching its peak around $x = 1$. Now we can calculate the localization loss by FocalL1 loss, $L_{Loc} = \sum_{i \in \{x, y, w, h\}} L_f(|B_i - B_i^{gt}|)$, where B is the regression result and B^{gt} is the regression target.

4.2. Focal-EIOU Loss

To enable the EIOU loss focus on high-quality examples, one can naturally consider replacing x in Eq. (9) with the EIOU loss. However, we observe that the above combination doesn't work well. The analysis is as follows.

Given the offset $\ell_1(B_i) = |B_i - B_i^{gt}|$, the gradient of the FocalL1 loss is $\frac{\partial L_f(\ell_1(B_i))}{\partial B_i} = \frac{\partial L_f}{\partial \ell_1} \frac{\partial \ell_1}{\partial B_i}$, where $\frac{\partial \ell_1}{\partial B_i}$ is a constant equals 1 or -1 . Thus, even the offset is small, $\frac{\partial L_f}{\partial \ell_1}$ can also bring enough gradients to make the model continuously optimized. However, if we replace the offset $\ell_1(B_i)$ with $L_{EIOU}(B, B^{gt})$, the gradient can be calculated as $\frac{\partial L_f}{\partial L_{EIOU}} \frac{\partial L_{EIOU}}{\partial B_i}$. Here, the $\frac{\partial L_{EIOU}}{\partial B_i}$ is not a constant value any more. Moreover, it will be very small in our empirical studies as the L_{EIOU} approaches to zero, while the $\frac{\partial L_f}{\partial L_{EIOU}}$ is also near to zero at that time. Thus, after the multiplication, the overall gradient will be even more smaller, which weakens the effect of reweighting on the boxes with small L_{EIOU} . To tackle this problem, we use the value of IOU to reweight the EIOU loss and get Focal-EIOU loss as follows

$$L_{\text{Focal-EIOU}} = \text{IOU}^\gamma L_{\text{EIOU}}, \quad (10)$$

where $\text{IOU} = |A \cap B| / |A \cup B|$ and γ is a parameter to control the degree of inhibition of outliers. We also try other forms of the reweighting process in Section 5.4.4, while we find Eq. (10) achieves superior performance.

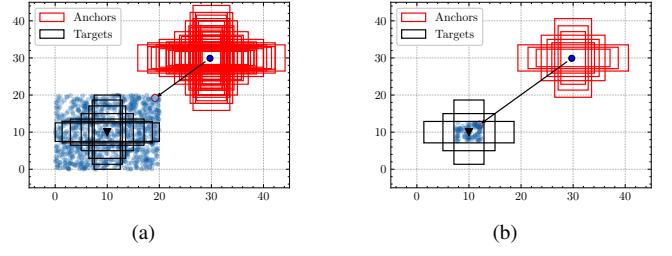


Figure 6: Simulation setup: (a) Setup 1: 7 target box and $1000 \times 7 \times 7$ anchors. (b) Setup 2: 3 target box and $100 \times 3 \times 3$ anchors.

5. Experiments

5.1. Datasets and Evaluation Metrics

We conduct experiments with both synthetic and real datasets. For the synthetic data, we conduct two simulation experiments to respectively study the superiorities of the EIOU and Focal-EIOU loss, as well as the importance of EEM. As shown in Figure 6(a), we randomly generate 1000 points within a 20×20 box. Each point has a set of 7×7 anchors with different aspect ratios (1:4, 1:3, 1:2, 1:1, 2:1, 3:1 and 4:1) and different scales (50, 67, 75, 100, 133, 150 and 200). The blue points denote the central points of anchors, where the red rectangles illustrate the 7×7 scales of the anchors around one of the 1000 blue central points. We also have 7 target boxes locating at (10,10). These target boxes all have a fixed scale 100 but different aspect ratios (1:4, 1:3, 1:2, 1:1, 2:1, 3:1 and 4:1). To emphasize the importance of EEM, we initialize higher quality anchors than those in Figure 6(a). We further constrain to sample anchors within a smaller square (the blue area) around the target locations, so that the anchors will have heavy overlaps with targets, which simulate the common situations in real scenarios. As depicted in Figure 6(b), 100 points are generated within a square whose center point is (10,10) and the side length is 2.5. Each point has a set of 3×3 anchors with different aspect ratios (1:3, 1:1, 3:1) and different scales (50, 100, 150). Targets boxes have three aspect ratios (1:3, 1:1, 3:1) and a fixed scale 100. The simulation algorithm is depicted in Algorithm 1. We go through all the anchors and regress them to each target. For specific anchor $B_{n,s}$ and target B_i^{gt} , we regress anchor $B_{n,s}^{t-1}$ to $B_{n,s}^t$ according to the gradient of the loss L w.r.t $B_{n,s}^{t-1}$ at iteration t . The performance of the regression process is evaluated with ℓ_1 loss and IOU metric.

We also present the experimental results on the bounding box detection track of the challenging COCO 2017 dataset [16]. We use the COCO train-2017 split (115k images) for training and report the ablation studies on the val-2017 split (5k images). The COCO-style Average Precision (AP) is chosen as the main evaluation metric.

5.2. Implementation Details

For fair comparisons, all experiments are implemented with PyTorch [20]. The backbones used in the experiments are publicly available. For most experiments on COCO 2017 dataset,

Algorithm 1 Simulation Experiments

Input: $A = 7$ or 3 represents simulation setup 1 or setup 2. $\{\{B_{n,s}\}_{s=1}^S\}_{n=1}^N$ denotes all the anchors at N points, where $S = A * A$ is the number of combinations of different areas and aspect ratios. $\{B_i^{gt}\}_{i=1}^A$ is the set of target boxes in $(10, 10)$ with an area of 100.

Output: IOU $\mathbf{I} \in \mathcal{R}^{T \times N \times S \times A}$ of each target-anchor box pair and regression error $\mathbf{E} \in \mathcal{R}^T$ in each iteration, where T is the maximal iteration and N is the number of generated points.

```

1:  $(T, \mathbf{E}, \mathbf{I}) \leftarrow (200, \mathbf{0}, \mathbf{0})$ 
2: for  $t = 1$  to  $T$  do
3:   for  $n = 1$  to  $N$  do
4:     for  $s = 1$  to  $S$  do
5:       for  $i = 1$  to  $A$  do
6:         if  $t \leq 0.8T$  then  $\mu = 0.1$ 
7:         else if  $t \leq 0.9T$  then  $\mu = 0.01$ 
8:         else  $\mu = 0.001$ 
9:         end if
10:         $\nabla B_{n,s}^{t-1} = \partial L(B_{n,s}^{t-1}, B_i^{gt}) / \partial B_{n,s}^{t-1}$ 
11:         $B_{n,s}^t = B_{n,s}^{t-1} + \mu \nabla B_{n,s}^{t-1}$ 
12:         $\mathbf{E}(t) = \mathbf{E}(t) + |B_{n,s}^t - B_i^{gt}|$ 
13:         $\mathbf{I}(t, n, s, i) = \text{IOU}(B_{n,s}^t, B_i^{gt})$ 
14:      end for
15:    end for
16:  end for
17: end for
18: Return  $\mathbf{E}, \mathbf{I}$ 

```

we use ResNet-50 backbone and run 90k iterations. For comparisons with previous methods we run 90k iterations with various backbones. We train detectors with 4 GPUs (4 images per GPU), adopting the stochastic gradient descent (SGD) optimizer with the initial learning rate 0.01 and decaying it by a factor of 0.1 at 50k, 70k and 80k. We doesn't following previous settings that decay the learning rate twice because EIOU loss brings larger gradients and high learning rate leads to unstable training. The default weight for BBR is set to 1.0 for ℓ_n -norm losses and 2.5 for IOU-based losses. All other hyperparameters follow the settings in ATSS [12] if not specifically noted.

In order to avoid the slow convergence speed in the early training period due to reweighting, we use the sum of weights in each batch to normalize the Focal-EIOU loss. Formally,

$$L_{\text{Focal-EIOU}} = \frac{\sum_{i=1}^n W_i \cdot L_{\text{EIOU}_i}}{\sum_{i=1}^n W_i}, \quad (11)$$

where n is the number of anchor-target pairs in each batch. L_{EIOU_i} and W_i are the EIOU loss of anchor-target pair i and the corresponding weight.

5.3. Simulation Experiments

Figure 7(a) and Figure 7(b) show the simulation results when most of the anchors are low quality examples. It verifies that the EIOU loss has a faster convergence speed and better regression accuracy than the IOU, GIOU and CIOU losses. Note

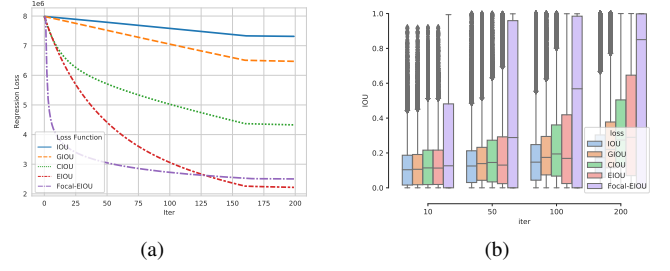


Figure 7: Simulation experimental results 1: (a) Regression error sum curves of different loss functions. (2) Variation trend of box plot of IOU with different loss functions. The Focal-EIOU loss with parameters $\gamma = 0.5$.

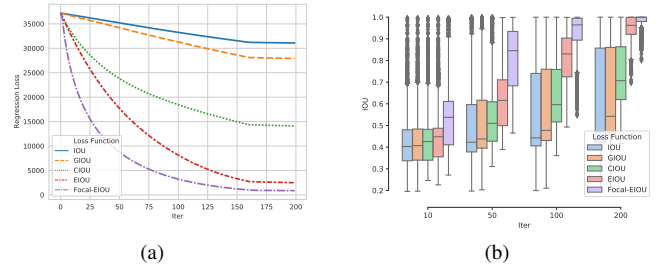


Figure 8: Simulation experimental results 2: (a) Regression error sum curves of different loss functions. (2) Variation trend of box plot of IOU with different loss functions. The Focal-EIOU loss with parameters $\gamma = 0.5$.

that, the regression error of Focal-EIOU loss is larger than the EIOU loss, which is depicted in Figure 7(a). While in Figure 7(b), the Focal-EIOU loss is less concerned about hard examples and these examples bring lots of regression errors for the Focal-EIOU loss. However, both the number and quality of high-quality examples of the Focal-EIOU loss are much higher than the other four kinds of loss functions.

Figure 8(a) and Figure 8(b) demonstrates the importance of EEM. The Focal-EIOU loss shows its extraordinary dominance over other IOU based losses. It not only has the fastest convergence speed and lowest regression error (Figure 8(a)), but also improves the quality of these high-quality examples at a speed far beyond other loss functions. Compared with the EIOU loss, the Focal-EIOU loss has a longer tail, while the mean value of IOU in Figure 8(b) is much higher. In other words, although the Focal-EIOU loss has some low-quality regressed anchors, it indeed has much more high-quality regressed anchors than the EIOU loss.

From the above simulation experiments, both the EIOU and the Focal-EIOU loss have achieved faster convergence speed. The Focal-EIOU loss has lower localization errors due to the reweighting on those high-quality examples.

5.4. Ablation Experiments

5.4.1. Overall Ablation Studies

To demonstrate the effectiveness of each proposed component, we report the overall ablation studies in Table 1. The FocalL1 loss improves the box AP from 35.9% to 36.5%. The

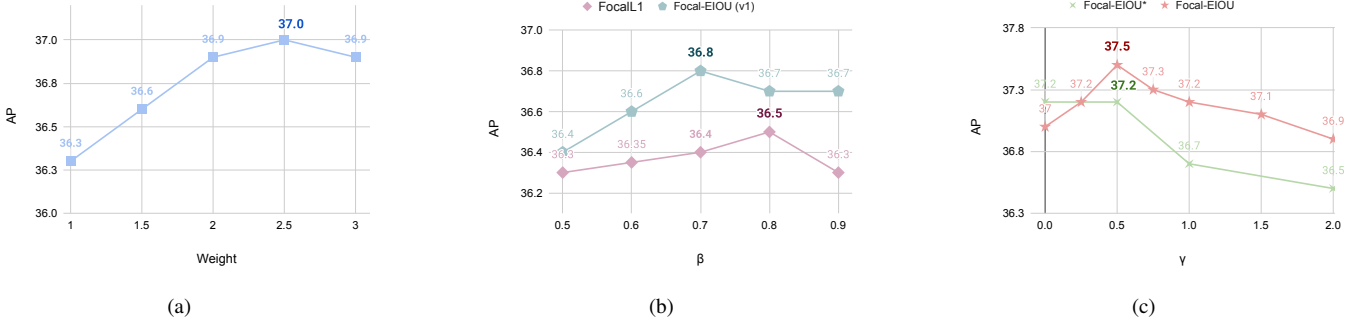


Figure 9: Performance of methods with different values of parameters. (a) The EIOU loss with different weights for BBR. (b) The FocalL1 and Focal-EIOU (v1) loss with different β . (c) The Focal-EIOU and Focal-EIOU* loss with different γ .

Method	AP	AP ₅₀	AP ₇₅	AP _S	AP _M	AP _L
Baseline	35.9	55.2	38.4	21.2	39.5	48.4
IOU	36.5	55.6	38.9	20.9	40.1	48.0
GIOU	36.5	55.6	39.0	20.7	40.2	48.2
CIOU	36.7	55.7	39.2	20.6	40.4	49.0
FocalL1	36.5	55.8	38.9	21.2	39.8	48.8
EIOU	37.0	55.7	39.5	20.7	40.5	49.5
Focal-EIOU (v1)	36.8	55.4	39.5	20.9	40.0	49.1
Focal-EIOU	37.5	56.1	40.0	21.1	40.9	49.8

Table 1: Overall ablation studies on COCO val-2017.

EIOU loss brings 1.1% higher box AP than the ResNet-50 FPN RetinaNet baseline. Directly applying Eq. (9) to the EIOU loss (namely use the EIOU loss as x in Eq. (9)), we can get Focal-EIOU (v1) and it doesn't work well. However, the Focal-EIOU loss in Eq. (10) brings reasonable gains, improving the baseline's AP by 1.6%. We also conduct experiments with the IOU, GIOU, CIOU and EIOU losses in Table 1. For fair comparisons, we set the weight for BBR to 2.5. Experimental results show that the performance of other IOU-based losses is inferior to the proposed method. Then we conduct detailed ablations for each block and hyper-parameter.

5.4.2. Effect of the Tradeoff Weight

We first verify the effects of the weight for BBR, where the weight here controls the balance between the classification loss and BBR loss in object detection. Figure 9(a) shows that tuning the weight can improve the performance with gains of 1.1% AP. The performance with a loss weight larger than 2.5 starts to drop down. These results indicate that these outliers have a negative impact on the training process and we do not fully utilize the potential of the model architecture.

Setting	AP	AP ₅₀	AP ₇₅	AP _S	AP _M	AP _L
Baseline	35.9	55.5	38.4	21.2	39.5	48.4
BalancedL1	36.3	55.3	38.8	20.5	39.3	48.5
FocalL1	36.5	55.8	38.9	21.2	39.8	48.8

Table 2: Ablation studies of the FocalL1 loss on COCO val-2017.

5.4.3. Ablation Studies on FocalL1 Loss

As shown in Figure 9(b), we test different β of the FocalL1 loss. Generally speaking, setting a larger β will further suppress the gradients of low-quality examples, but increase the gradients of high-quality examples. Finally, we find that setting $\beta = 0.8$ achieves the best trade-off and 36.5% AP, which is 0.6% higher than the ResNet-50 FPN RetinaNet baseline. We also reimplement the BalancedL1 loss with the superior parameters proposed in the previous work [19] and it brings 0.4% improvement on AP (Table 2). These experimental results show that the FocalL1 loss makes the model better.

5.4.4. Ablation Studies on Focal-EIOU Loss.

To illustrate the improvements brought by different methods for reweighting the EIOU loss, we compare three reweighting methods here. We firstly show that the form of the FocalL1 loss is not suitable, namely using the EIOU loss as x in Eq. (9). The experimental results are shown in Figure 9(b). As we mentioned before, applying the FocalL1 loss directly to the EIOU loss leads to the reduction of the high-quality examples' gradients, which is not suitable for and thus cannot improve the performance of the EIOU loss.

We then use the focal loss [15] to reweight the EIOU loss and get the Focal-EIOU* loss, i.e., $L_{\text{Focal-EIOU}^*} = -(1 - \text{IOU})^\gamma \log(\text{IOU})\text{EIOU}$. Originally, the focal loss works well when facing the extreme foreground-background class imbalance. Results in Figure 9(c) show that although we can gain performance improvements, it quickly decrease with the increase of γ . The reason is that we cannot suppress the gradients of hard examples in such an extreme way due to their effectiveness in the BBR process.

Finally we evaluate the proposed method in Eq. (10). Figure 9(c) shows that compared to the focal loss, the proposed

Method	Backbone	AP	AP ₅₀	AP ₇₅	AP _S	AP _M	AP _L
Faster R-CNN [23]	ResNet-50-FPN	37.3	58.2	40.3	21.3	40.9	48.0
Faster R-CNN*	ResNet-50-FPN	38.9	59.1	42.4	21.2	41.1	50.2
Faster R-CNN [23]	ResNeXt-101-32x4d-FPN	41.2	62.1	45.1	24	45.5	53.5
Faster R-CNN*	ResNeXt-101-32x4d-FPN	42.4	63.1	46.8	24.2	46.3	54.1
Mask R-CNN [10]	ResNet-50-FPN	38.2	58.8	41.4	21.9	40.9	49.5
Mask R-CNN*	ResNet-50-FPN	39.6	59.3	41.7	22.4	41.5	51.1
Mask R-CNN [10]	ResNeXt-101-32x4d-FPN	41.9	62.5	45.9	24.4	46.3	54.0
Mask R-CNN*	ResNeXt-101-32x4d-FPN	43.0	63.1	46.1	24.4	47.3	56.1
RetinaNet [15]	ResNet-50-FPN	35.9	55.2	38.4	21.2	39.5	48.4
RetinaNet*	ResNet-50-FPN	37.5	56.1	40.0	21.3	40.9	49.8
RetinaNet [15]	ResNeXt-101-32x4d-FPN	40.8	60.9	43.7	22.9	44.5	54.6
RetinaNet*	ResNeXt-101-32x4d-FPN	41.8	61.4	44.7	21.7	45.0	55.2
ATSS [29]	ResNet-50-FPN	39.1	57.6	42.1	22.9	42.8	51.1
ATSS*	ResNet-50-FPN	39.7	57.9	45.7	22.6	43.2	51.8
ATSS	ResNeXt-64x4d-101-DCN	50.7	68.9	56.3	33.2	52.9	62.2
ATSS*	ResNeXt-64x4d-101-DCN	51.4	69.3	57.3	32.8	53.4	64.2
PAA [12]	ResNet-50-FPN	40.3	57.6	43.9	23.0	44.9	54.0
PAA*	ResNet-50-FPN	40.8	57.9	44.7	22.9	45.3	54.9
PAA [12]	ResNeXt-64x4d-101-DCN	51.4	69.7	57.0	34.0	53.8	64.0
PAA*	ResNeXt-64x4d-101-DCN	52.3	70.2	58.1	33.2	54.3	66.2
DETR [3]	ResNet-50	42.0	62.4	44.2	20.5	45.8	61.1
DETR*	ResNet-50	43.2	62.5	45.3	21.1	46.1	62.7

Table 3: The performance when incorporating the Focal-EIOU loss with different SOTA models. * indicates using the Focal-EIOU loss instead of their original losses.

method brings more stable improvement. Larger γ brings stronger suppression on hard examples and may retard the convergence speed. This is also the reason why the performance is poorer than the baseline when $\gamma = 2.0$. We find that setting $\gamma = 0.5$ achieves the best trade-off and use it as the default value for further experiments.

5.5. Incorporations with State-of-the-Arts

In this subsection, we evaluate the Focal-EIOU loss by incorporating it into popular object detectors including Faster R-CNN [23], Mask R-CNN [10], RetinaNet [15], PAA [12] and ATSS [29], and DETR [3]. Results in Table 3 show that training these models by the Focal-EIOU loss can consistently improve their performance compared to their own regression losses. Compared to other models, the ATSS and PAA attain relatively small improvements. There are two reasons: (i) The ATSS and PAA both use the GIOU loss with carefully adjusted parameters. These parameters may not be suitable for the proposed Focal-EIOU loss. (ii) Both ATSS and PAA have the reweighting processes on their own localization losses (In PAA, it is the predicted IOUs with corresponding target box. In ATSS, it is the centerness scores when using the centerness prediction). Although these reweighting methods limit the improvement brought by the Focal-EIOU loss, they confirm the necessity of EEM.

Finally, we emphasize that L_{IOU} , L_{GIOU} only achieves 0.1% AP improvement (Table 5 in [24]) and L_{CIOU} achieves 0.72% AP improvement (Table.3 in [30]) when using Faster R-CNN as the baseline. By comparison, the Focal-EIOU loss brings

1.6% AP improvement. It is a relatively huge performance gain, verifying our method is simple but efficient. Recent work Generalized Focal Loss [14] consists of two parts: Quality Focal Loss (QFL) and Distribution Focal Loss (DFL). The former is not relevant to the BBR. The latter is an efficient loss for BBR, while it also ignored the importance of EEM. From Table 3 in [14], we can see that using DFL only improves the performance of ATSS from 39.2% to 39.5% AP while our Focal-EIOU loss brings 0.6% AP improvement.

5.6. Discussion on Focal-EIOU loss and error set analysis

Figure 10(a) shows that one can easily find more accurate boxes with higher prediction confidence. However, Focal-EIOU loss is more sensitive to large elements, it occasionally assigns wrong boxes near the large element, which is shown in Figure 10(b). Besides, in terms of the small elements, Focal-EIOU loss is a little inferior to the original IOU loss. In Figure 10(c), Focal-EIOU loss assigns blurry boxes with lower prediction confidence to the small surfboard. Nevertheless, Focal-EIOU loss performs much better for medium and large objects. Samples in Figure 11 show that the proposed Focal-EIOU loss performs better on medium and large objects and may ignore or assign low-quality boxes and low-confidence predictions to small objects.

6. Conclusion

This paper takes a thorough analysis of BBR for object detection and find that the potential of the loss function has not been

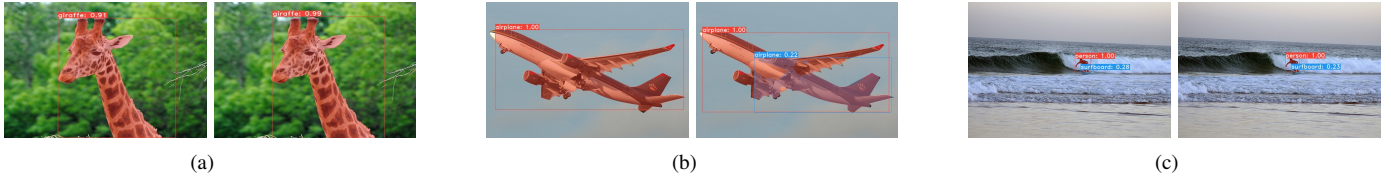


Figure 10: Detection examples using Faster R-CNN trained on COCO 2017 dataset. Visualization samples are chosen from COCO test-2014. (a,b): Left: \mathcal{L}_{CIOU} , right: $\mathcal{L}_{Focal-EIOU}$. (c): Left: \mathcal{L}_{IOU} , right: $\mathcal{L}_{Focal-EIOU}$

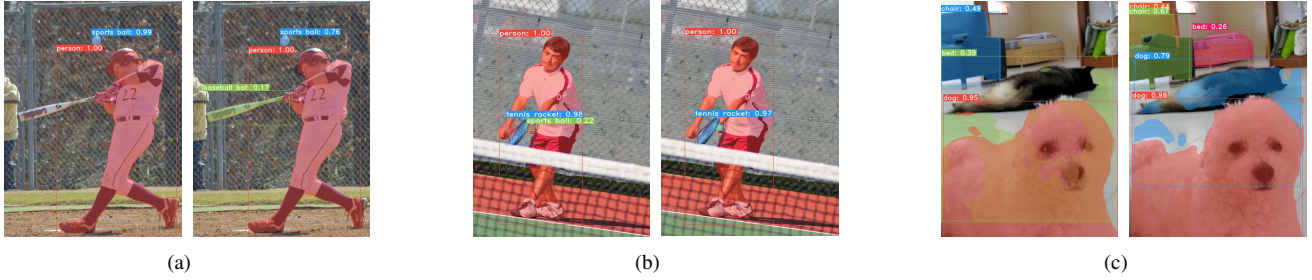


Figure 11: Detection examples using Faster R-CNN trained on COCO 2017 dataset. Visualization samples are chosen from COCO test-2014. Left: \mathcal{L}_{CIOU} , right: $\mathcal{L}_{Focal-EIOU}$.

fully exploited. The first reason is that existing loss functions all have some drawbacks, hindering the regression of bounding boxes from being guided correctly. Secondly, existing studies mostly neglect the importance of effective example mining of BBR. Therefore, low-quality examples contribute excessively large gradients and further limit the performance of BBR. Based on the observation, we propose the Focal-EIOU loss to tackle existing losses' defects and balance the gradients derived by the high and low-quality examples. Extensive experiments on both the synthetic and COCO dataset show that the Focal-EIOU loss brings significant and consistent improvements with a number of state-of-the-art models.

References

- [1] Sara Beery, Guanhang Wu, V. Rathod, Ronny Votel, and Jonathan Huang. Context r-cnn: Long term temporal context for per-camera object detection. *2020 IEEE/CVF Conference on Computer Vision and Pattern Recognition (CVPR)*, pages 13072–13082, 2020. 2
- [2] Zhaowei Cai and Nuno Vasconcelos. Cascade r-cnn: Delving into high quality object detection. In *CVPR*, 2018. 1
- [3] Nicolas Carion, Francisco Massa, Gabriel Synnaeve, Nicolas Usunier, Alexander Kirillov, and Sergey Zagoruyko. End-to-end object detection with transformers. In *European conference on computer vision*, pages 213–229. Springer, 2020. 1, 2, 8
- [4] Kean Chen, Weiyao Lin, Jianguo Li, John See, Ji Wang, and Junni Zou. Ap-loss for accurate one-stage object detection. *IEEE Transactions on Pattern Analysis and Machine Intelligence*. 2
- [5] Zhiming Chen, Kean Chen, Weiyao Lin, John See, Hui Yu, Yan Ke, and Cong Yang. Piou loss: Towards accurate oriented object detection in complex environments, 2020. 2
- [6] P. F. Felzenszwalb, R. B. Girshick, D. McAllester, and D. Ramanan. Object detection with discriminatively trained part-based models. *IEEE Transactions on Pattern Analysis and Machine Intelligence*, 32(9):1627–1645, 2010. 2
- [7] Spyros Gidaris and Nikos Komodakis. Locnet: Improving localization accuracy for object detection. In *Proceedings of the IEEE Conference on Computer Vision and Pattern Recognition (CVPR)*, June 2016. 2
- [8] Ross Girshick. Fast r-cnn. In *Proceedings of the IEEE International Conference on Computer Vision (ICCV)*, December 2015. 1, 2
- [9] Ross Girshick, Jeff Donahue, Trevor Darrell, and Jitendra Malik. Rich feature hierarchies for accurate object detection and semantic segmentation. In *Proceedings of the IEEE Conference on Computer Vision and Pattern Recognition (CVPR)*, June 2014. 2
- [10] Kaiming He, Georgia Gkioxari, Piotr Dollár, and Ross Girshick. Mask r-cnn. In *Proceedings of the IEEE International Conference on Computer Vision (ICCV)*, Oct 2017. 1, 2, 8
- [11] K. He, X. Zhang, S. Ren, and J. Sun. Spatial pyramid pooling in deep convolutional networks for visual recognition. *IEEE Transactions on Pattern Analysis and Machine Intelligence*, 37(9):1904–1916, 2015. 2
- [12] Kang Kim and Hee Seok Lee. Probabilistic anchor assignment with iou prediction for object detection. In *ECCV*, 2020. 2, 6, 8
- [13] Sven Kosub. A note on the triangle inequality for the jaccard distance. *Pattern Recognition Letters*, 120:36 – 38, 2019. 3
- [14] Xiang Li, Wenhai Wang, Lijun Wu, Shuo Chen, Xiaolin Hu, Jun Li, Jinhui Tang, and Jian Yang. Generalized focal loss: Learning qualified and distributed bounding boxes for dense object detection. *arXiv preprint arXiv:2006.04388*, 2020. 8
- [15] Tsung-Yi Lin, Priya Goyal, Ross Girshick, Kaiming He, and Piotr Dollár. Focal loss for dense object detection. In *Proceedings of the IEEE International Conference on Computer Vision (ICCV)*, Oct 2017. 1, 2, 7, 8
- [16] Tsung-Yi Lin, Michael Maire, Serge Belongie, James Hays, Pietro Perona, Deva Ramanan, Piotr Dollár, and C. Lawrence Zitnick. Microsoft coco: Common objects in context. In David Fleet, Tomas Pajdla, Bernt Schiele, and Tinne Tuytelaars, editors, *Computer Vision – ECCV 2014*, pages 740–755, Cham, 2014. Springer International Publishing. 2, 5
- [17] Wei Liu, Dragomir Anguelov, Dumitru Erhan, Christian Szegedy, Scott Reed, Cheng-Yang Fu, and Alexander C. Berg. Ssd: Single shot multibox detector. In Bastian Leibe, Jiri Matas, Nicu Sebe, and Max Welling, editors, *Computer Vision – ECCV 2016*, pages 21–37, Cham, 2016. Springer International Publishing. 2
- [18] Jiangmiao Pang, Kai Chen, Jianping Shi, Huajun Feng, Wanli Ouyang, and Dahua Lin. Libra r-cnn: Towards balanced learning for object detection. In *Proceedings of the IEEE/CVF Conference on Computer Vision and Pattern Recognition (CVPR)*, June 2019. 2
- [19] Jiangmiao Pang, Kai Chen, Jianping Shi, Huajun Feng, Wanli Ouyang, and Dahua Lin. Libra r-cnn: Towards balanced learning for object detection. In *IEEE Conference on Computer Vision and Pattern Recognition*, 2019. 2, 4, 7
- [20] Adam Paszke, Sam Gross, Soumith Chintala, Gregory Chanan, Edward

- Yang, Zachary DeVito, Zeming Lin, Alban Desmaison, Luca Antiga, and Adam Lerer. Automatic differentiation in pytorch. 2017. [5](#)
- [21] Q. Qian, L. Chen, H. Li, and R. Jin. Dr loss: Improving object detection by distributional ranking. In *2020 IEEE/CVF Conference on Computer Vision and Pattern Recognition (CVPR)*, pages 12161–12169, Los Alamitos, CA, USA, jun 2020. IEEE Computer Society. [2](#)
- [22] Joseph Redmon, Santosh Divvala, Ross Girshick, and Ali Farhadi. You only look once: Unified, real-time object detection. In *Proceedings of the IEEE Conference on Computer Vision and Pattern Recognition (CVPR)*, June 2016. [2](#)
- [23] Shaoqing Ren, Kaiming He, Ross Girshick, and Jian Sun. Faster r-cnn: Towards real-time object detection with region proposal networks. In C. Cortes, N. D. Lawrence, D. D. Lee, M. Sugiyama, and R. Garnett, editors, *Advances in Neural Information Processing Systems* 28, pages 91–99. Curran Associates, Inc., 2015. [2](#), [8](#)
- [24] Hamid Rezatofighi, Nathan Tsoi, JunYoung Gwak, Amir Sadeghian, Ian Reid, and Silvio Savarese. Generalized intersection over union: A metric and a loss for bounding box regression. In *Proceedings of the IEEE/CVF Conference on Computer Vision and Pattern Recognition (CVPR)*, 2019. [2](#), [3](#), [8](#)
- [25] Abhinav Shrivastava, Abhinav Gupta, and Ross Girshick. Training region-based object detectors with online hard example mining. In *Proceedings of the IEEE Conference on Computer Vision and Pattern Recognition (CVPR)*, June 2016. [2](#)
- [26] Yue Wu, Yinpeng Chen, Lu Yuan, Zicheng Liu, Lijuan Wang, Hongzhi Li, and Yun Fu. Rethinking classification and localization for object detection. In *Proceedings of the IEEE/CVF Conference on Computer Vision and Pattern Recognition (CVPR)*, June 2020. [2](#)
- [27] Jiahui Yu, Yuning Jiang, Zhangyang Wang, Zhimin Cao, and Thomas Huang. Unitbox: An advanced object detection network. In *Proceedings of the 24th ACM International Conference on Multimedia, MM '16*, page 516–520, New York, NY, USA, 2016. Association for Computing Machinery. [1](#), [2](#), [3](#)
- [28] Hongkai Zhang, Hong Chang, Bingpeng Ma, Naiyan Wang, and Xilin Chen. Dynamic R-CNN: Towards high quality object detection via dynamic training. *arXiv preprint arXiv:2004.06002*, 2020. [1](#), [2](#), [4](#)
- [29] Shifeng Zhang, Cheng Chi, Yongqiang Yao, Zhen Lei, and Stan Z. Li. Bridging the gap between anchor-based and anchor-free detection via adaptive training sample selection. In *CVPR*, 2020. [2](#), [8](#)
- [30] Ping Wang Zhaohui Zheng, Jinze Li Wei Liu, and Dongwei Ren Rongguang Ye. Distance-iou loss: Faster and better learning for bounding box regression. In *The AAAI Conference on Artificial Intelligence (AAAI)*, 2020. [2](#), [3](#), [8](#)